Accepted Manuscript

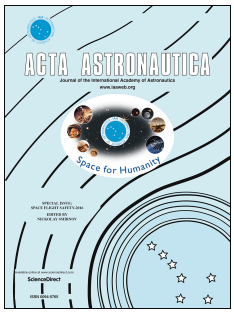

Supersonic jet and nozzle flows in uniform-flow and free-vortex aerodynamic windows of gas lasers

V.N. Emelyanov, A.V. Pustovalov, K.N. Volkov

PII: S0094-5765(18)32042-3

DOI: https://doi.org/10.1016/j.actaastro.2019.01.014

Reference: AA 7280

To appear in: *Acta Astronautica*

Received Date: 11 December 2018

Revised Date: 9 January 2019

Accepted Date: 10 January 2019

Please cite this article as: V.N. Emelyanov, A.V. Pustovalov, K.N. Volkov, Supersonic jet and nozzle flows in uniform-flow and free-vortex aerodynamic windows of gas lasers, *Acta Astronautica* (2019), doi: https://doi.org/10.1016/j.actaastro.2019.01.014.

Supersonic jet and nozzle flows in uniform-flow and free-vortex aerodynamic windows of gas lasers

V.N. Emelyanov[1], A.V. Pustovalov[1], K.N. Volkov[2,*]

[1]Baltic State Technical University, 190005, St Petersburg, Russia

[2]Kingston University, SW15 3DW, London, United Kingdom

Abstract

The mathematical models and computational tools for design, analysis and predictions of supersonic jet and nozzle flows in the aerodynamic windows of high-power gas lasers are considered. The steady-state Euler equations describing strong shock waves, contact discontinuities, rarefaction waves and their interactions are solved with the finite-volume solver and space-marching method. The results of numerical simulation of steady-state supersonic flows of inviscid compressible gas in nozzles and under- and over-expanded jets are obtained and analyzed for different pressure ratios in the laser cavity and ambient atmosphere. The flowfields corresponding to the uniform velocity profile and free-vortex velocity profile in the outlet nozzle boundary are compared. Nozzle profiling tools are developed on the basis of numerical solution of a sequence of direct problems. The aerodynamic performance of the window is evaluated in terms of the simulated laser cavity pressure and plenum pressure of the free-vortex supply nozzle. The pressure support characteristic for the aerodynamic window is established by determining the ambient to cavity pressure ratio over a range of aerodynamic window supply pressures.

Keywords

Flight safety; Gas laser; Aerodynamic window; Supersonic flow; Nozzle; Jet; Space-marching method

1 Introduction

Simulation of high-speed flows plays an important role in space flight safety [1, 2]. High-speed flows significantly affect the performance and robustness of optical sensors and optical windows. The compressible flow and aerodynamic heating of the window material induce large density gradients on a shock wave in front of the optical window. These density gradients impose refractive index variations, and the shock wave and aerodynamic flow around the optical window act as an aerodynamic lens with refraction index gradients. Use of traditional optical windows is also limited if the intensity of laser beam is sufficiently high that the energy cannot pass through a solid window without catastrophic disruption of both window and laser beam [3, 4].

The aerodynamic windows have been designed to separate two regions between which high-intensity laser beam propagates. Instead of separating the different regions with a solid window, an aerodynamic window separates them with a transverse stream of air. High-pressure air is expanded through a nozzle to create shock and rarefaction waves on either

*Corresponding author: k.volkov@kingston.ac.uk

side of the window. This sets up a strong pressure gradient across the window (transverse to the flow direction). If the respective high- and low-pressures are matched to the external pressures on either side of the window, flow does not occur across the window. Aerodynamic windows are widely used in high-power gas lasers to extract the energy of the laser beam from the resonator chamber through a non-absorbing flow, thus maintaining a required pressure difference between the laser cavity and the surrounding [5]. The practical applications of aerodynamic windows vary from stationary applications at sea level to supersonic applications at various altitudes. The flow in the aerodynamic window is adjusted to accommodate changing external conditions (external pressure variations due to altitude and vehicle speed or geometry).

The laser beam is extracted from the low-pressure environment through an optical duct and enters into the supersonic flow region of a nozzle via an oblique opening in the duct. The beam crosses the oblique shock wave formed by the wedge surface of the opening and passes along the nozzle centerline through the nozzle throat, its subsonic section and into the atmosphere. A device for extraction of energy of laser beam includes a plane nozzle producing a supersonic jet in the window aperture whose external boundary is located on the source side of the atmosphere (high-pressure region) and whose internal boundary is located on the source side of the optical resonator chamber (low-pressure region), and a plane diffuser receiving the jet flow (Figure 1). To reduce the mass flow rate of the working gas through the nozzle and to improve pressure recovery in the diffuser, aerodynamic windows use profiled nozzles and nozzles of specific design. In unform-flow aerodynamic windows, the duct for extraction of laser energy from the resonator chamber and the jet flow are intersected at certain angle. Different shock wave structures significantly affecting the quality of the optical beam are formed depending on the design features of the nozzle and pressure difference. Variations of the density are responsible for the variations of the refractive index of the medium and optical quality of the window.

The existing designs of aerodynamic windows of gas lasers with a transverse supersonic jet are divided into two groups, aerodynamics windows with a uniform flow on the nozzle outlet and free-vortex aerodynamic windows (in the free vortex $vr = \text{const}$, where v is the velocity and r is the radial coordinate). In the aerodynamic windows with a uniform flow, curvature of the transverse supersonic jet is attained in a rarefaction wave, inclined shock wave or combination of rarefaction wave and inclined shock wave [6–10]. In the free-vortex aerodynamic windows, a supersonic flow with a velocity distribution typical for a free vortex is formed in the nozzle outlet [11–18]. The gas in the free-vortex aerodynamic window moves in concentric circles with a velocity inversely proportional to the radius of the streamline, and the pressure difference is maintained by centrifugal forces. In practice, $\overline{p} = 1.5 \ldots 15$, where $\overline{p} = p_2/p_1$.

The principle of the aerodynamic window is based on the force balance between the inertial forces of the gas flow and the pressure forces across the aperture area. The angular change in jet velocity vector is inversely proportional to the required mass flow rate. The mass flow rate is also proportional to the pressure in the plenum at the entrance of the free-vortex supply nozzle. A diffuser is located opposite to the nozzle exit. This device has to take the gas jet to recover the pressure and the exhaust the used gas to the ambient atmosphere. A constant area diffuser is usually sufficient because the required pressure recovery is low.

The main characteristic of an aerodynamic window, on which the possibility of its practical use depends, is optical quality. When solving problems of focusing and transmitting radiation to remote objects, it is necessary to ensure an acceptable level of beam divergence at the outlet from the optical path of the laser device. The optical quality of the aerodynamic windows associated with minimizing the distortion of the amplitude and phase characteristics

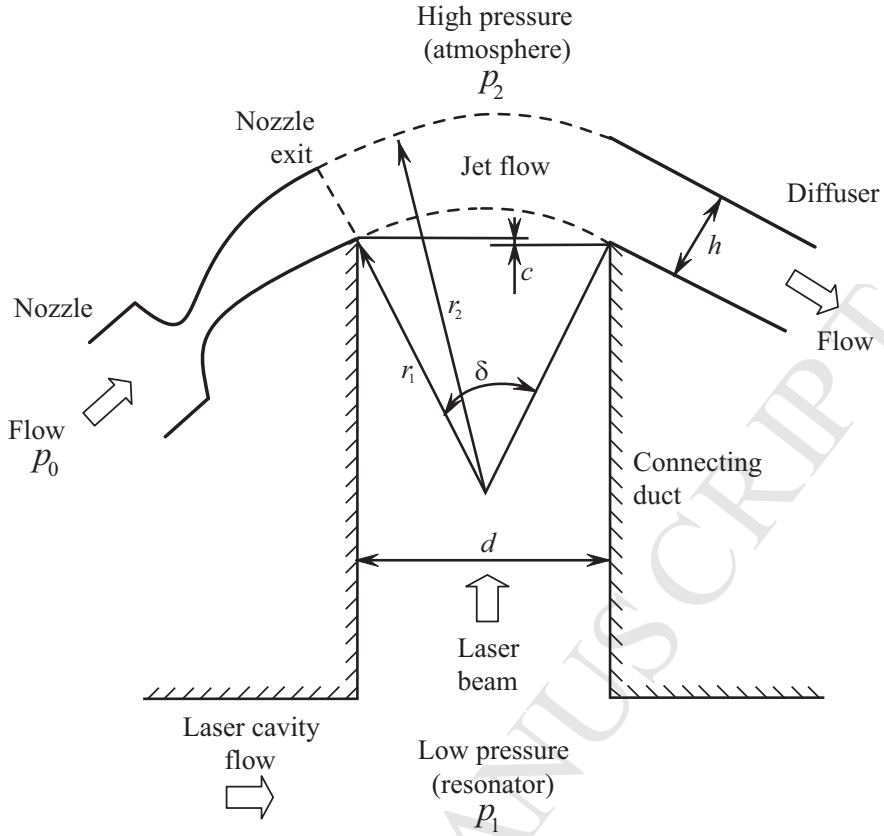

Figure 1. Aerodynamic window of gas laser

of the wave front when radiation passes through the medium plays an important role in practical applications [5].

Jets with a uniform velocity distribution on the nozzle outlet are studied in [6, 7]. Implementation of this configuration requires a large mass flow rate of air. The change in the momentum of the jet due to pressure difference is accompanied by the formation of a shock wave and rarefaction wave leading to the degradation of quality of optical beam. To preserve the quality of the optical beam, nozzles creating a velocity distribution corresponding to the free vortex in the outlet section are used [11, 12]. The mass flow rate required for the operation of these devices and the optical quality of the window have been investigated as a function of operating conditions and the window design [6, 7, 11, 12]. Experiments are performed in [9] to define operating conditions which cause a minimal degradation in the quality of a laser beam transmitted through the window. It has been shown that with proper choice of design variables the beam quality degradation caused by the aerodynamic window is less than 10%. Design of a supersonic free-vortex aerodynamic window ensuring optical quality and fluid-mechanical sealing of a simulated laser cavity for active controlling of the gas flow in the aerodynamic window by adjusting part of the diffuser is discussed in [14]. The free-vortex aerodynamic window uses a supply nozzle which provides a non-uniform supersonic jet well suited to large amount of flow turning.

The study [15] describes the design procedure of two-dimensional supersonic free-vortex nozzle, and demonstrates the operating conditions of the window taking into account the phase transition of the working fluid in the nozzle expansion process and the operating conditions of the supersonic diffuser. A free-vortex supersonic nozzle with large asymmetry and minimum length is developed in [16]. The validity of the nozzle contour is confirmed by a comparison between the density distribution obtained from experimental measurements and isentropic calculations. The pressure characteristics of the aerodynamic window strongly

depend on the diffuser geometry and its configuration. It is found that the optical quality of the aerodynamic window is determined mostly by the shear flow instability on the atmospheric side of the supersonic jet.

One way of improvement of the optical quality consists in density drop decrease by working gas heating [17]. Optimum heating of the jet gas improves the optical quality of aerodynamic windows. For ideal gas, it is possible to receive as much as large pressure difference, however for real gas a pressure difference more than 50 is difficult to achieve. To achieve the pressure ratio 100 in free-vortex single-stage aerodynamic window the method of stabilizing of boundary layer is proposed [18]. The gas is decelerated in the diffuser and is exhausted into the atmosphere straightly. The pressure recovery improvement is achieved by using the boundary layer blowing inside the diffuser. Only 10% of total mass flow is used for boundary layer blowing.

Aero-optical phenomena involve the propagation of transmitted beams, such as lasers and imaging beams. The main reasons for the change in the refractive index are variations of the density and gas composition due to diffusion and gas dynamic processes. Changes in the phase of the wave front are divided into steady state and unsteady. The steady-state distortions of the wave front are due to the average non-uniform distribution of the refractive index, and the unsteady distortions are related to turbulent fluctuations of the density [19]. The joint influences of the non-uniform compressed flowfield and the aerodynamically heated optical window on imaging quality of an optical system are discussed in [20].

In the aerodynamic windows with a transverse jet, optical distortions due to the heating of the gas by laser radiation are negligible for any power of the extracted laser radiation. To assess optical distortions in practice, the approximation of steady-state flow of a inviscid compressible gas is applied. To make design decisions, it is necessary to develop efficient and robust computational tools to analyze the characteristics of aerodynamic windows and to facilitate nozzle profiling that form jets with required properties [21]. In evaluating the performance of the aerodynamic window, the main areas of concern are the amount of mass flow required by the aerodynamic window to produce the desired momentum change, the ability of the aerodynamic window to transmit the laser beam with minimum optical quality degradation, and the effectiveness of the aerodynamic window in preventing leakage of the surrounding gases into the laser cavity.

In this study, computational tools are developed to carry out simulation of supersonic flows in nozzles and jets with unusual properties that are realized in uniform-flow and free-vortex aerodynamic windows. Numerical method is based on the finite volume method and space-marching method. Steady-state supersonic flows of an inviscid compressible flows in nozzles and jets are simulated, and nozzle profiling tools are created.

2 Governing equations

The aerodynamic window uses the segment of the free vortex bounded by the inner radius, r_1, and outer radius, r_2, and inclined within the flow turning angle, δ (Figure 1). By selecting the velocity and total pressure in combination with the free-vortex velocity and pressure distributions, the static pressure at the segment boundaries is matched to the laser cavity pressure and ambient pressure. With the flow conditions matched in this manner, the flow over aperture is turned gradually by the Mach lines of the supersonic flow. Since the flow turning is maintained by the Mach waves present at the nozzle outlet, strong shock waves are avoided. This offers the potential for increased flow turning and reduced gas supply requirements.

Atmospheric air is entrained along the outer jet boundary and ingested into the diffuser. The outer diffuser wall is designed so that its leading edge lies on a line extended from the downstream edge of the aperture and parallel with the laser beam path. A small distance between lower wall of the nozzle and lower wall of the diffuser, c, has a great impact on the laser cavity pressure ratio. The width of the diffuser channel, h, is larger that the width of the nozzle outlet boundary.

For simulation of steady-state two-dimensional compressible inviscid gas flows conservation form of the Euler equations written in a Cartesian frame of reference (x, y) is used

$$\frac{\partial \boldsymbol{F}(\boldsymbol{U})}{\partial x} + \frac{\partial \boldsymbol{G}(\boldsymbol{U})}{\partial y} = 0. \tag{1}$$

The total energy per unit volume for a perfect gas is found from the equation

$$e = \frac{p}{\gamma - 1} + \frac{1}{2}\rho(u^2 + v^2).$$

Vector of conservative flow variables and flux vectors are

$$\boldsymbol{U} = \begin{pmatrix} \rho \\ \rho u \\ \rho v \\ e \end{pmatrix}, \quad \boldsymbol{F} = \begin{pmatrix} \rho u \\ \rho u u + p \\ \rho u v \\ (e + p)u \end{pmatrix}, \quad \boldsymbol{G} = \begin{pmatrix} \rho v \\ \rho v u \\ \rho v v + p \\ (e + p)v \end{pmatrix}.$$

Here, ρ is the density; u and v are the velocity components in the Cartesian directions x and y; p is the static pressure; e is the total energy per unit volume; γ is the ratio of specific heat capacities at constant pressure and constant volume.

For supersonic gas flows without recirculation regions, Euler equations (1) are hyperbolic with respect to the space coordinate which is close to the main flow direction [22, 23]. If the flow is supersonic along one Cartesian coordinate, the Euler equations (1) are hyperbolic along this coordinate. In particular, the Euler equations are hyperbolic if $u^2 + v^2 > c^2$. Hyperbolicity in x direction takes place if $u^2 > c^2$, and hyperbolicity along y direction takes place if $v^2 > c^2$. The case of x hyperbolicity is considered for clarity.

In a hyperbolic case, an initial boundary problem (Cauchy problem) is formulated. Initial data on the supersonic inlet boundary $x = x_0$ are required to start space-marching calculations. The characteristic analysis shows that all flow quantities should be specified in the section $x = x_0$ (outlet boundary of the nozzle). In the addition to the initial data, different boundary conditions can be considered. No-penetration boundary condition is imposed on a solid wall, where the tangential velocity component is zero. The main flow quantities are prescribed on the relevant boundary to generate an incident shock wave. For a symmetric problem, the symmetry boundary conditions are applied to the centreline.

The assumption of a fully attached flow (hyperbolicity in the main flow direction) is significant becoming inappropriate in many real cases. The separated jet wave structures vary greatly from the fully attached model predictions. In addition to this, the assumption of inviscid flow excludes the mixing and boundary layer flows that occur at the jet boundaries. These assumptions cause the numerical results to differ considerably from the observed behaviour of real flows. Although these limitations affect the accuracy of the predicted flowfield, they are mostly prominent far downstream of the jet inception. For the supersonic jet, its spreading from mixing is relatively small.

3 Numerical method

A number of explicit and implicit space-marching methods based on high-order TVD or ENO finite-difference schemes have been developed to solve steady-state Euler equations (1). These methods have been efficiently applied to the simulation of steady-state flows with strong discontinuities described by the Euler equations which are hyperbolic in the entire flow domain [23].

The explicit non-iterative space-marching procedure proposed in [22] is used to solve Euler equations (1) on a structured mesh with uniform mesh steps Δx and Δy in the Cartesian directions x and y. For supersonic inviscid gas flows without separation in streamwise direction, the Euler equations (1) are hyperbolic in the main flows direction. Assuming that the mesh lines $x = \text{const}$ are close to the main flow direction, the derivatives in the streamwise direction (derivatives with respect to the marching coordinate) are evaluated by explicit first-order backward finite differences.

The computational procedure includes the reconstruction of the flow quantities on the faces of control volumes using cell-average values and the solution of Riemann problem. The solution of Riemann problem consists of two waves (shock waves or rarefaction waves) separated by the contact discontinuity and regions of uniform flow. Initial conditions on a cell boundary are $\boldsymbol{U}_i^k = \text{const}$ if $y \leqslant y_{i+1/2}$ and $\boldsymbol{U}_{i+1}^k = \text{const}$ if $y > y_{i+1/2}$, where $\boldsymbol{U}_i$ is the cell-average flow quantities $\boldsymbol{U}$. The vector of flow quantities computed from the Riemann problem on cell boundary $i + 1/2$ is referred to as $\boldsymbol{U}_{i+1/2}$.

The finite volume scheme for equations (1) has the form

$$\frac{\boldsymbol{F}_i^{k+1} - \boldsymbol{F}_i^k}{\Delta x} + \frac{\boldsymbol{G}_{i+1/2} - \boldsymbol{G}_{i-1/2}}{\Delta y} = 0, \tag{2}$$

where $\boldsymbol{G}_{i\pm1/2} = \boldsymbol{G}(\boldsymbol{U}_{i\pm1/2})$. The superscript $k = 0, 1, \ldots$ corresponds to the flow quantities on a space layer k in x direction.

A wide range of finite-difference schemes is available to evaluate derivatives in the crossflow direction. To capture flowfields with strong shock waves and contact discontinuities, the second-order TVD scheme is applied to the discretization of crossflow derivatives in the equation (2). The conservative nature and second-order accuracy of the scheme allow to resolve flow discontinuities without non-physical oscillations and with a small numerical dissipation resulting in the spreading of shock waves and contact discontinuities over a several mesh cells.

The corrected numerical flux for the second-order TVD scheme is computed as

$$\boldsymbol{F}_{i+1/2} = \frac{1}{2}\left(\boldsymbol{G}_i^k + \boldsymbol{G}_{i+1}^k\right) + \frac{1}{2}\left|A_{m+1/2}^k\right|\left(\boldsymbol{F}_i^k - \boldsymbol{F}_{i+1}^k\right),$$

where $A = (\partial \boldsymbol{G}/\partial \boldsymbol{U})(\partial \boldsymbol{F}/\partial \boldsymbol{U})^{-1}$. The stability condition is

$$C = \max|\lambda_\pm|\frac{\Delta x}{\Delta y} \leqslant 1.$$

The eigenvalues of the Jacobian matrix are

$$\lambda_\pm = \frac{uv \pm c(u^2 + v^2 - c^2)^{1/2}}{u^2 - c^2}.$$

Speed of sound is found from the relationship

$$c = \left[(\gamma - 1)h_0 - \frac{1}{2}(\gamma - 1)(u^2 + v^2)\right]^{1/2},$$

where h_0 is the total enthalpy.

4 Space-marching method

A physical flow region Ω shown in the Figure 2a is a connected domain bounded by two straight lines, one for inlet boundary and another one for outlet boundary, and two piecewise smooth curves, Γ_1 and Γ_2, representing free boundaries (upper and lower boundaries of a jet) or solid walls. Initial data on the inlet boundary include distributions of flow quantities on the inlet boundary of flow domain, a_1. It is assumed that the flow is fully supersonic on the outlet boundary (Euler equations remain hyperbolic), and boundary conditions are not imposed on this boundary.

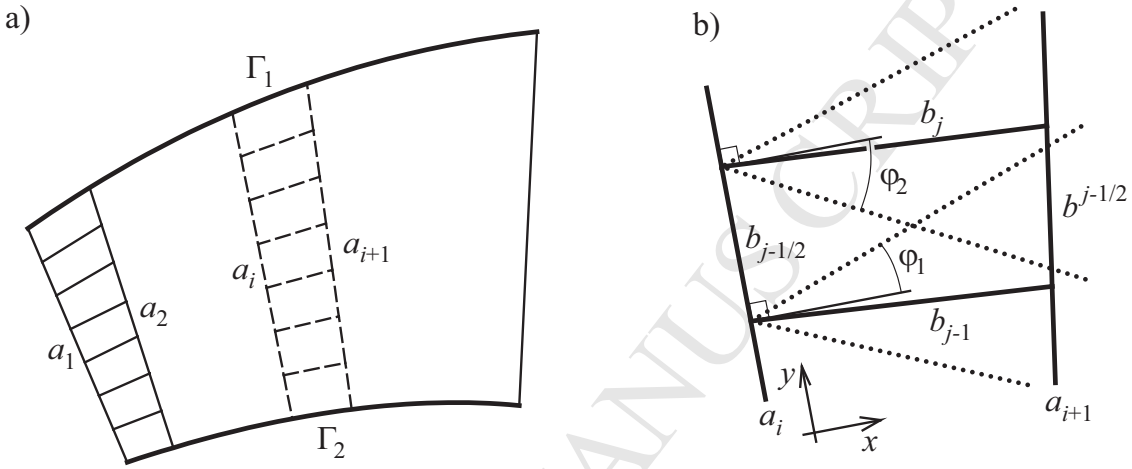

Figure 2. Flow domain (a) and control volume (b)

The calculations start from the space layer a_i where flow quantities are assumed to be given. The space layer a_i is sub-divided into n equal straight segments $b_{j-1/2}$. Average values of the flow quantities (for example, the pressure p_{j-1} and the density ρ_{j-1}) are determined on each straight segment using flow quantities from the previous space layer. A new space layer a_{i+1} is constructed and sub-divided into n equal straight segments $b^{j-1/2}$. The nodes located on the space layers a_i and a_{i+1} are connected by the straight segments b_j, and the control volume with boundaries b_{j-1}, $b^{j-1/2}$, b_j and $b_{j-1/2}$ is formed. The control volume is shown in the Figure 2b (solid lines), where φ_1 and φ_2 are the angles determining the wave propagation directions resulting from the interaction of two uniform supersonic flows (dotted lines). Once the flow quantities on the layer a_{i+1} have been computed, the next space layer is constructed, and the corresponding flow quantities are determined. The process is repeated until the parameters in the entire flow domain are calculated.

Space-marching method is based on the integration of Euler equation (1) in the main flow direction using the scheme (2). The flow quantities on the space layer a_{i+1} consisting of a number of straight segments $b^{j-1/2}$ are found from the computed flow quantities on the space layer a_i consisting of a number of straight segments $b_{j-1/2}$. The finite-volume scheme is written as

$$(\boldsymbol{F}h_y - \boldsymbol{G}h_x)^{j-1/2} = (\boldsymbol{F}h_y - \boldsymbol{G}h_x)_{j-1/2} + (\boldsymbol{F}h_y - \boldsymbol{G}h_x)_j + (\boldsymbol{F}h_y - \boldsymbol{G}h_x)_{j-1}\,, \qquad (3)$$

where h_x and h_y are the projections of cell sides on the Cartesian directions x and y.

The flow quantities on the boundaries b_j and b_{j-1} are determined by the solution of the problem of interaction of two supersonic uniform plane flows (Riemann problem). Waves resulting from the interaction of two uniform flows in each point on a space layer a_i propagate in the main flow direction towards the layer a_{i+1}. The resulting flow is shown in the

Figure 3. Dashed line corresponds to the contact discontinuity, and dotted lines correspond to either the shock wave or the rarefaction wave (the wave nature depends on the ratio of flow parameters on segments $b_{j-1/2}$ and $b_{j+1/2}$).

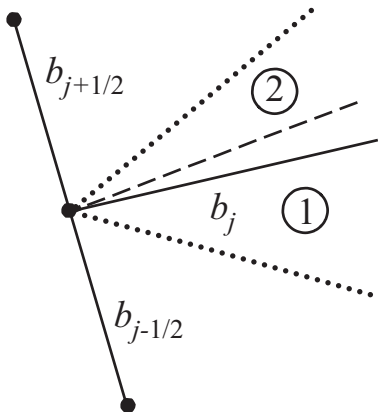

Figure 3. Riemann problem

A maximum possible integration step in the streamwise direction is found from the Courant–Friedrichs–Lewy condition. The distance to the corresponding segment $b^{j-1/2}$ (segment belonging to the space layer a_{i+1}), at which the stability condition is satisfied, is found from the equation

$$\Delta S = \left[(h_x^2 + h_y^2)(\mathrm{M}_{j-1/2}^2 - 1)\right]^{1/2},$$

where h_x and h_y are the projections of the segment $b_{j-1/2}$ on Cartesian directions x and y, and $\mathrm{M}_{j-1/2}$ is the Mach number.

The angle φ_k determining the direction of the wave propagation resulting from the interaction of two uniform supersonic flows and corresponding to the segment $b_{<k>}$ of the space layer, where k is the local index of the segment $b_{j-1/2}$ (the index 1 corresponds to the segment b_{j-1}, and the index 2 corresponds to the segment b_j) is found from the equation

$$\varphi_k = \mathrm{atan}(\zeta_{j-1/2}) \pm \sigma_k,$$

where

$$\sigma_k = \begin{cases} \mathrm{asin}(1/\mathrm{M}_{j-1/2}) & \text{if } p_{j-1/2} \geqslant p_{<k>}, \\ \mathrm{asin}\left[\dfrac{\gamma+1}{2\gamma \mathrm{M}_{j-1/2}^2}\left(\dfrac{p_{<k>}}{p_{j-1/2}} + \dfrac{\gamma-1}{\gamma+1}\right)\right]^{1/2} & \text{if } p_{j-1/2} < p_{<k>}. \end{cases}$$

Here, $\zeta_j = u_j/v_j$. A plus sign corresponds to $k = 1$, and a minus sign corresponds to $k = 2$.

The flow quantities p and ζ on the contact discontinuity are found using iterative approach

$$p^{(n+1)} = \left[\alpha_1^{(n)} + \alpha_2^{(n)}\right]^{-1}\left[\beta_1^{(n)}\zeta_{j-1/2} - \beta_2^{(n)}\zeta_{j+1/2} + \alpha_1^{(n)}p_{j-1/2} + \alpha_2^{(n)}p_{j+1/2}\right];$$

$$\zeta^{(n+1)} = \beta_1^{(n)}\zeta_{j-1/2} - \alpha_1^{(n)}\left(p^{n+1} - p_{j-1/2}\right) = \beta_2^{(n)}\zeta_{j+1/2} + \alpha_2^{(n)}\left(p^{n+1} - p_{j+1/2}\right).$$

The superscript n correspond to the iteration number. The coefficients α_k and β_k are calculated as

$$\alpha_k = \begin{cases} \dfrac{1}{2}\left(s_k + s_{<k>}\right) & \text{if } p_k \leqslant p_{<k>}, \\ \beta_k g_k & \text{if } p_k > p_{<k>}; \end{cases}$$

$$\beta_k = \begin{cases} 1 & \text{if } p_k \leqslant p_{<k>}, \\ \dfrac{1}{1 \pm \zeta_{<k>}[g_k(p_k - p_{<k>})]} & \text{if } p_k > p_{<k>}. \end{cases}$$

Here

$$s = \frac{1+\zeta^2}{\rho W^2}\left(\mathrm{M}^2 - 1\right)^{1/2}, \quad g_k = \left[\frac{2\gamma \mathrm{M}^2_{<k>} p_{<k>}}{(\gamma-1)p_{<k>} + (\gamma+1)p_k} - 1\right]^{1/2}.$$

The local index $\langle 1 \rangle$ corresponds to the segment $b_{j-1/2}$, and the local index $\langle 2 \rangle$ corresponds to the segment $b_{j+1/2}$. A plus sign corresponds to the index $k = 1$, and a minus sign corresponds to the index $k = 2$.

The flow quantities are found from the following relationships:

— flow density

$$\rho_k = \rho_{<k>} \begin{cases} \left(\dfrac{p}{p_{<k>}}\right)^{1/\gamma} & \text{if } p \leqslant p_{<k>}, \\ \dfrac{(\gamma-1)p_{<k>} + (\gamma+1)p}{(\gamma+1)p_{<k>} + (\gamma-1)p} & \text{if } p > p_{<k>}; \end{cases}$$

— flow speed

$$W_k = \left(\frac{\gamma+1}{\gamma-1}c_*^2 - \frac{2\gamma}{\gamma-1}\frac{p}{\rho_{<k>}}\right)^{1/2};$$

— flow velocity components in the coordinate directions

$$u_k = \frac{W_k}{(1+\zeta^2)^{1/2}}, \quad v_k = \zeta u_k;$$

— Mach number

$$\mathrm{M}_k = \frac{W_k}{(\gamma p_k/\rho_k)^{1/2}}.$$

The critical speed of sound is

$$c_* = \left(\frac{\gamma-1}{\gamma+1}W^2_{<k>} + \frac{2\gamma}{\gamma+1}\frac{p_{<k>}}{\rho_{<k>}}\right)^{1/2}.$$

The parameter $\chi \in (0,1)$ shows the position of the segment $b^{j-1/2}$ (segment belonging to the space layer a_{i+1}), where the stability condition is satisfied. The value $\chi = 0$ corresponds to the position of the space layer a_i, and the value $\chi = 1$ corresponds to the position of the space layer a_{i+1}.

Calculations are implemented in a sequence of several steps: the distance ΔS is calculated and the space layer a_{i+1} is positioned; the parameters p and ζ are computed; the angles φ_1 and φ_2 are determined; the position of the space layer a_{i+1} is refined if required; the position of the space layer a_{i+1} is changed if $\chi < 1$ otherwise calculations come back to the previous step, and the flow quantities on the segments b_j and $b^{j-1/2}$ are determined if $\chi > 1$; the space layer a_i is moved to a new position a_{i+1}. The required number of steps is made in the streamwise (marching) direction.

5 Under- and over-expended jets

Simulations of steady-state flows of inviscid compressible gas in the supersonic plane jets are performed for two cases corresponding to different velocity profiles on the nozzle outlet. The case 1 corresponds to the uniform velocity distribution, and the case 2 corresponds to the free-vortex velocity distribution. The calculations of supersonic jets in the aerodynamic windows of gas lasers separating the flow regions with different pressures are carried out for different pressure ratios. A simple structured mesh containing 101 nodes in y direction is used. A number of nodes in the streamwise direction depends on the length of the computational domain and case dependant. The structure of jet flow depends on the nozzle pressure ratio $\mathrm{NPR} = p_0/p_a$. It is defined as the ratio of nozzle inlet stagnation pressure, p_0, to atmospheric static pressure, p_a.

Initially, the operating NPR is insufficient for the Mach number to ever reach unity. The nozzle flow remains subsonic with the divergent section of the nozzle acting as a diffuser, slowing the flow down and increasing the static pressure. The NPR is increased to the point that there is sonic flow in the throat, but insufficient for supersonic flow at the nozzle outlet. A normal shock wave forms in the divergent section of the nozzle. Downstream of the shock wave, the flow is subsonic ($\mathrm{M} < 1$), and consequently the divergent section acts as a diffuser, slowing the flow down and increasing the static pressure. Further increase in NPR leads to the shock wave movement downstream through the divergent section of the nozzle. As the NPR is further increased, the flow becomes supersonic at the nozzle outlet.

For supersonic flows, the gas velocity exceeds the speed of sound, and the pressure difference between the jet outlet pressure and the surrounding pressure is possible at the nozzle exit, which then influences the downstream behavior of the jet [24]. For a fixed nozzle geometry, the flow is fully expanded if NPR is such that the jet exits with a pressure equal to that of the surrounding pressure (NPR is equal to the design value N). However, if the jet exit pressure is lower than the surrounding pressure, the jet is over-expanded. At over-expanded conditions, the wave pattern includes the formation of oblique and normal shock waves [25]. Oblique shock waves turn the flow inwards (concave deflection) whilst normal shock waves preserve the original flow direction. Both oblique and normal shock waves reduce the jet velocity and raise the static pressure. This pressure rise equalizes the jet outlet pressure to the surrounding pressure. The condition where the jet outlet pressure is larger than the surrounding pressure is under-expanded. At under-expanded conditions, an expansion fan forms at the nozzle outlet. The expansion fan turns the flow outwards (convex deflection) through a series of expansion waves that continuously decrease the jet pressure to that of the surroundings. Expansion fans and expansion waves are additionally characterized by a continuous increase in velocity [26].

The wave pattern of the supersonic jet is illustrated in the Figure 4 as the operating NPR increases. In the fragment a, oblique shock waves form at both sides of the nozzle exit as the static pressure at the outlet boundary is lower than ambient pressure [27]. In the

fragment b, the static pressure at the nozzle exit is equal to ambient pressure, consequently there are no waves, and the nozzle is operating at its correctly expanded conditions. In the fragment c, the static pressure at the nozzle outlet is greater than ambient pressure, consequently expansion fan waves form at the exit from both sides.

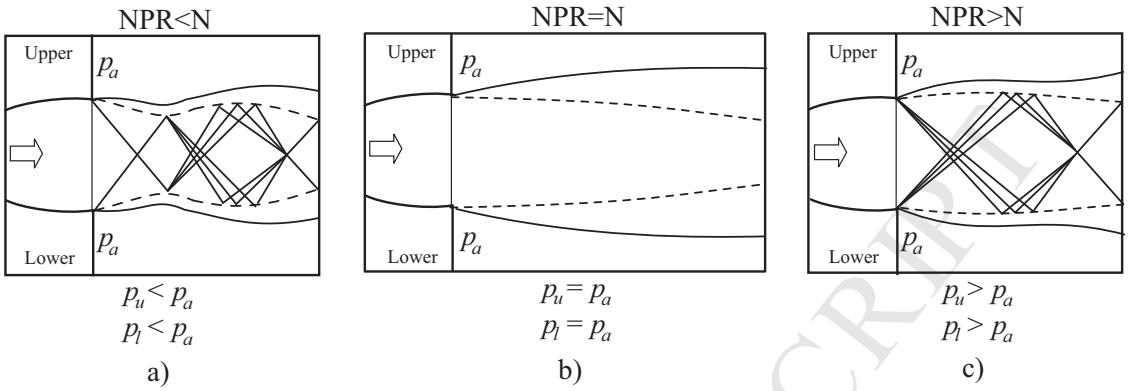

Figure 4. The operating conditions of free supersonic jet for symmetric nozzle ($p_l = p_u$)

For supersonic flow in non-symmetric nozzle, one side of the nozzle exit is designated as upper and the opposite side is designated as lower (Figure 5). The non-symmetric nozzle causes an outlet static pressure profile such that the static pressure at the lower side is always lower than the upper. If the static pressure at a side of the nozzle outlet is lower than ambient pressure then a shock wave forms on that side in order to increase the static pressure to ambient pressure. The operating condition of that side of the nozzle is referred to as over-expanded (fragment a). If the static pressure at a side of the nozzle outlet is equal to ambient pressure, then no waves form from that side, such an operating condition is referred to as correctly expanded (fragment b). The final possibility is for the static pressure at a side of the nozzle to be greater than ambient pressure. In this case, an expansion fan forms on that side of the nozzle outlet in order to reduce the static pressure to ambient pressure. This operating condition is referred to as under-expanded (fragment c). The operating condition definitions of over-expanded, correctly expanded and under-expanded are extended to the full jet in the case of a free jet issuing from a symmetrical nozzle as the static pressure on both sides of the nozzle outlet are identical.

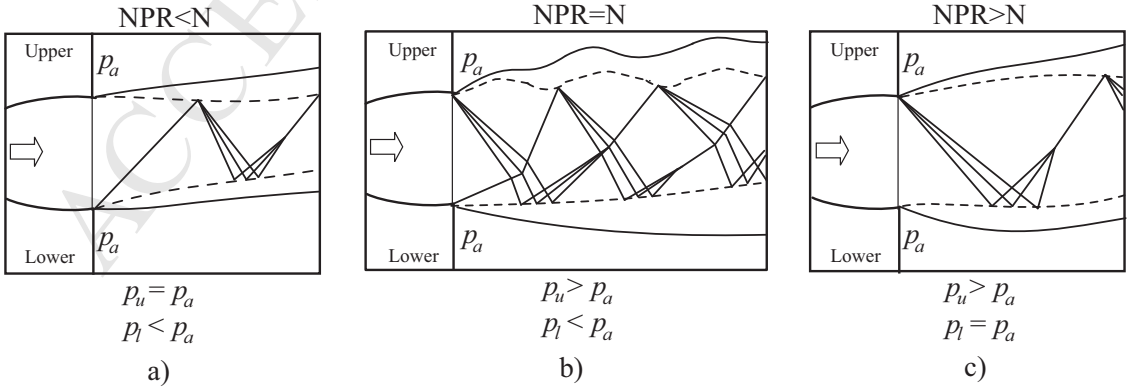

Figure 5. The operating conditions of free supersonic jet for non-symmetric nozzle (for the case considered, $p_l < p_u$)

Figure 4 and Figure 5 link the possible operating conditions and wave patterns of a supersonic jet issuing from both a symmetric and non-symmetric nozzle to the design NPR. For

the non-symmetric nozzle, the cases where both upper and lower sides of the jet are under-expanded and over-expanded are omitted for greater clarity (fragment a is over-expanded, fragment b is correctly expanded, fragment c is under-expanded). For the non-symmetric nozzle, the outlet static pressures at each side are different. Consequently, either side of the nozzle could potentially have different operating conditions. For a free jet issuing from non-symmetric nozzle, it is impossible for both sides to be operating at the correctly expanded condition (wave-free) simultaneously. In the event that a side of the nozzle is over-expanded or under-expanded, waves propagate through the jet, reflecting from the shear layer as opposites, with expansion fans reflecting as compression waves (coalescing to form shock waves), and shock waves reflecting as expansion fans. The term correctly expanded NPR is defined as the operating NPR at which there are no waves propagating from the nozzle outlet.

A complex wave pattern is formed downstream of the nozzle outlet for both over-expanded and under-expanded flows. The wave pattern is dictated by the initial wave form, the magnitude of the exit pressure difference and the wave interactions with boundaries. The interception of a wave with a boundary causes the wave to reflect. The form of the reflected wave depends on the type of boundary that is encountered. A solid boundary causes like reflection where an incident wave reflects as the same type of wave, ensuring that the streamline direction is maintained. At a free boundary, the converse wave form is reflected in order for the boundary pressure to remain constant. As a result of this, oblique shocks and compression waves are reflected as expansion waves, and expansion waves are reflected as compression waves that can coalesce (intersect and strengthen) to form a shock wave.

The structure of a plane supersonic jet with a uniform velocity profile on the inlet boundary is presented in the Figure 6. The nozzle pressure ratio is one for the upper half-space, and the jet is over-expanded for the lower half-space. At the high-pressure side of the nozzle outlet a curved shock wave originates. It is reflected on the opposite boundary as an expansion wave. The inner diffuser wall is located too close to the jet curvature so that the shock wave starts at the edge.

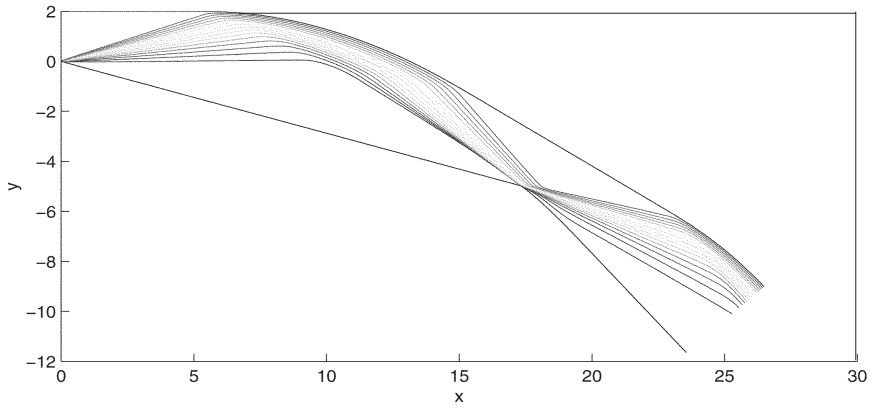

Figure 6. Density contours in the jet separating regions of low (lower side) and high (upper side) pressures

The flow structure presented in the Figure 7 corresponds to the jet with the nozzle pressure ratio of one for the upper half-space undergoing a positive pressure difference on a shock wave and separating the lower half-space with a higher pressure. Decreasing the nozzle pressure ratio in the upper half-space leads to the formation of a rarefaction wave on the upper edge and modification of the jet turning angle (Figure 8).

Flowfields in the over-expanded and under-expanded jets with different nozzle pressure ratios are presented in the Figure 9 and Figure 10. At under-expanded conditions, a primary expansion fan forms on the nozzle lip. Downstream of the nozzle outlet, the

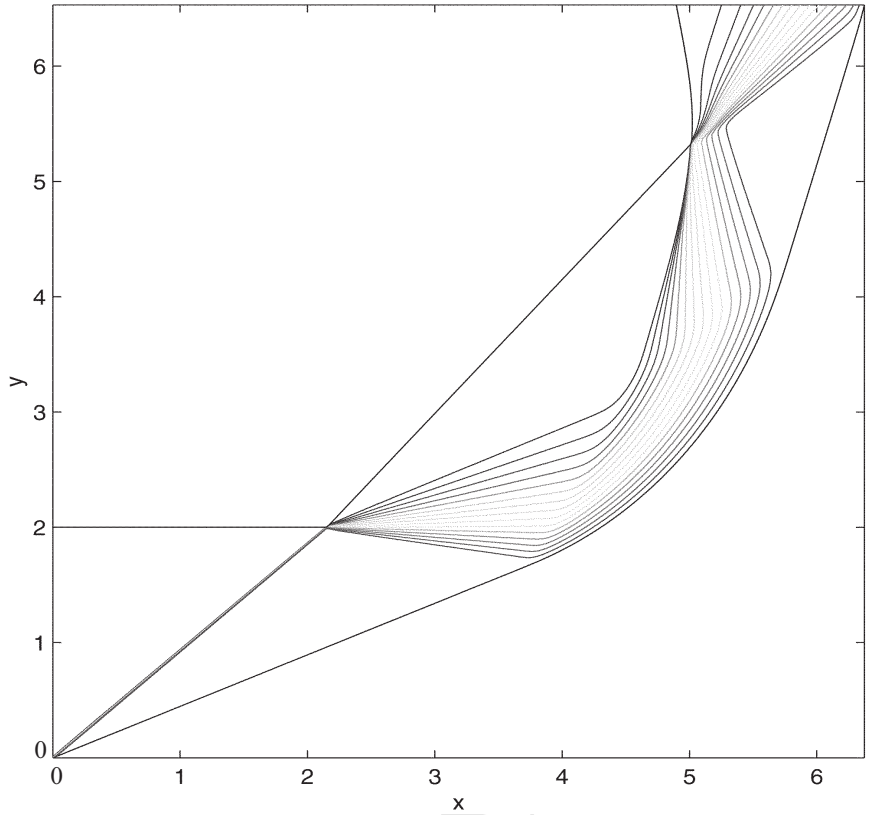

Figure 7. Density contours in the jets with correctly expanded (upper side) and over-expanded (lower side) boundaries

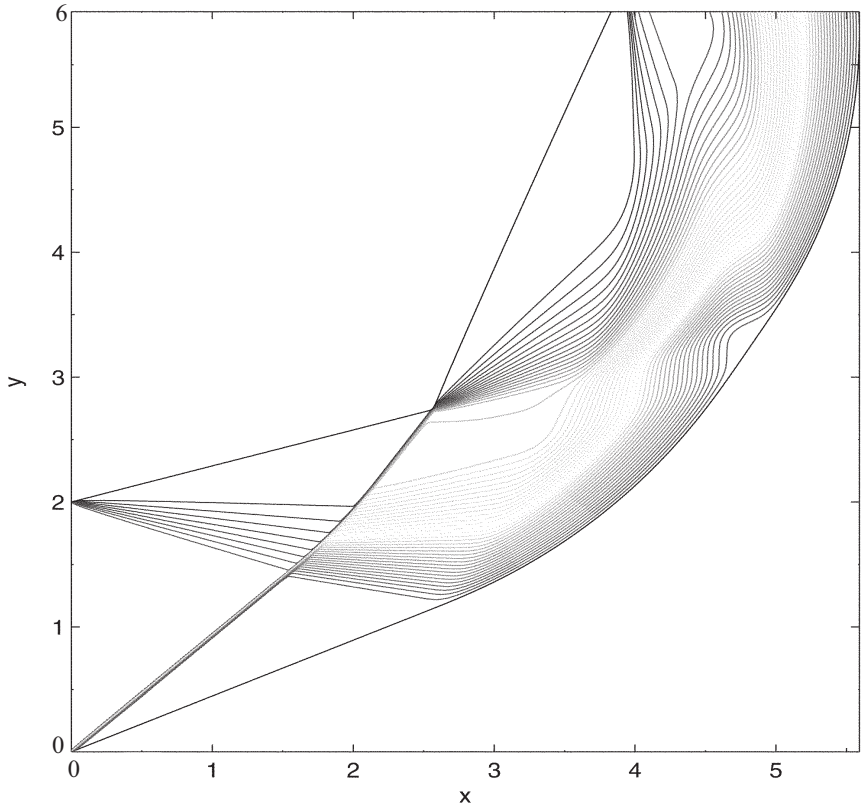

Figure 8. Density contours in the jet with under-expanded (upper side) and over-expanded (lower side) boundaries

primary expansion fan waves reflect as like on the curved wall and eventually reflect again as primary compression waves off the free boundary. The numerical results show how the curved boundary pressure decreases and increases as the flow passes through the expansion and compression waves. These plots highlight the increased strength of the expansion and compression as the nozzle pressure ratio becomes more under-expanded.

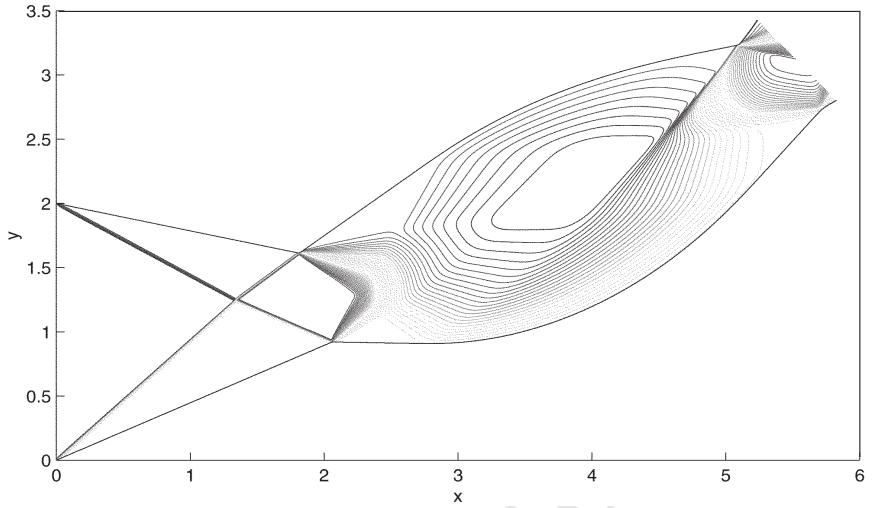

Figure 9. Density contours in the over-expanded jet for different degrees of over-expansion on the upper and lower boundaries

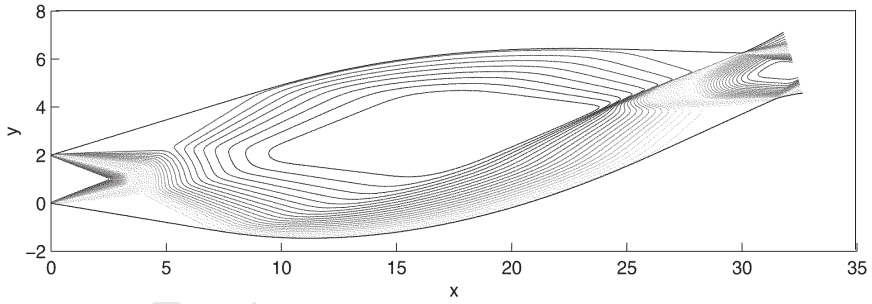

Figure 10. Density contours in the under-expanded jet for different degrees of under-expansion on the upper and lower boundaries

Flowfield in a jet with the inlet velocity profile corresponding to the free vortex is shown in the Figure 11. In this case, the streamlines represent circular arcs, and the pressure difference is maintained by centrifugal forces. Irrotational vortex flows is chosen for the target shear-flow velocity distribution as they have concentric circular streamlines. A convergent-divergent nozzle is then designed to achieve the specified outlet Mach distribution.

The uniform and free-vortex flows vary in wave structure and consequently shape. For the uniform velocity profile, a uniform characteristics field forms at the nozzle outlet due to the similarity in pressure between the jet and the surroundings. The free jet boundary for the uniform-flow initially follows a horizontal path and only begins to curve when the secondary expansion waves from the curved boundary intercept the free jet boundary. This creates a jet shape that deviates significantly from the ideal circular flow case. The secondary expansion waves form due to the convex deflection of the flow, and cause the flow to accelerate and the surface pressure to decrease. This creates a favorable streamwise pressure gradient. Downstream of the initial expansion, the secondary expansion waves reflect from the free boundary as secondary compression waves causing the surface pressure to increase and an

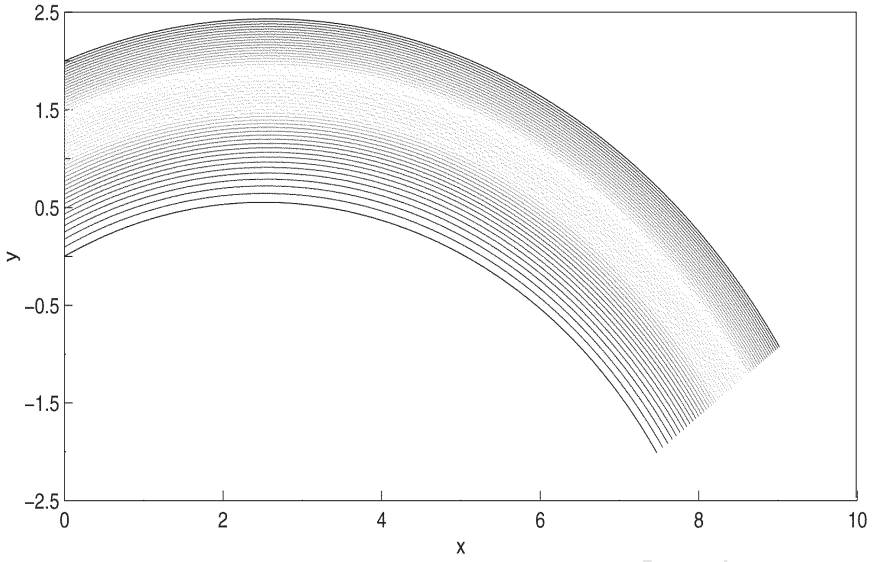

Figure 11. Density contours in the free-vortex jet

adverse streamwise pressure gradient to form. The secondary waves continue to reflect along the entire surface causing the reciprocating regions of expansion and compression.

The free-vortex jet results show different wave and pressure distributions. The free jet boundary for the shear-flow follows the ideal circular path. This is the intended result as the shear-flow Mach profile is matched explicitly to the curved surface radius. Unlike the uniform flow jet, the characteristic lines do not form a uniform field at the nozzle outlet. The presence of the shear-flow velocity gradient means there is a pressure gradient along the nozzle outlet. This pressure gradient along the nozzle outlet generates a characteristics field where the right-running characteristics are in compression and the left-running characteristics are in expansion. The expansion waves from the nozzle exit impinge on the free jet boundary, and cause it to deflect at the correct convex curvature. The compression waves from the nozzle outlet intercept with the curved boundary and exactly neutralize the acceleration effect of secondary expansion waves. The incident waves on the boundary eliminate the streamwise expansion and as a result, the surface pressure is constant for the entirety of the curved boundary and no streamwise pressure gradients are formed.

In comparison to the on-design nozzle, the most notable difference in wave structure is the introduction of primary expansion fans, customary with under-expanded flows. Downstream of the nozzle outlet, the primary expansion fan waves eventually reflect from the free jet boundary as primary compression waves that intersect, implying the formation of a shock wave in both flows.

6 Nozzle profiling

A non-symmetric nozzle is designed to produce a skewed velocity distribution at the nozzle outlet. If the high velocity and low pressure are on the one side, the radial pressure gradient acts to deflect the jet in that direction. The streamlines of an irrotational vortex flow are circular, and the velocity varies inversely with distance from the center of rotation. A jet with free-vortex velocity distribution flows around the circular surface without turning losses due to expansion waves.

The method of characteristics is widely used in the field of supersonic nozzle design [28]. Application of the method of characteristics to a flowfield yields characteristic directions

where compatibility equations are valid. These compatibility equations have one spatial derivative less than the starting governing equations. As a result, the user of the method of characteristics is only required to deal with simpler compatibility equations in the characteristic directions to evaluate a flowfield [29]. The streamline-tracing technique is a nozzle design method based on the streamlines of a known flowfield. Neglecting the effects of viscosity, a wall is inserted along any streamtube of a flow without modifying the characteristics of the streamtube. Surface shape design methods are mainly applied to the design of ducts and are characterized by the necessity for a target pressure distribution.

In free-vortex aerodynamic windows, the jet turns out to be strongly swirling in the direction normal to the flow velocity. The velocity in the jet changes in inverse proportion to the radius of curvature of the streamline. In an ideal case, there are no shock waves and the related pressure losses in the flow (flow is isentropic). Nozzles for aerodynamic windows of this type produce a free vortex whose parameters are determined by the working gas and pressure ratio in the flows separated by the window.

Supersonic nozzles are designed to produce outlet jet Mach number profiles, and therefore outlet pressure profiles matching that of an irrotational vortex (circular shear-flow). In the optimization procedure, the nozzle geometries are simulated with appropriate inlet boundary conditions. The resulting outlet velocities are then compared against the desired, and appropriate adjustments are made to the nozzle design input parameters. Use of the inviscid flow assumption provides a reasonable approximation for internal flow behavior at low computational cost compared to the solution of the viscous flow Navier–Stokes equations. This assumption although computationally inexpensive, is strictly valid only where viscous effects are negligible. In the non-symmetric nozzle, the flow on the lower wall inside the nozzle accelerates faster than the flow on the upper wall. This leads to the skewness of the velocity profile and adjustment of the radial pressure gradient at the nozzle outlet.

Nozzle profiling is a central problem to be solved when free-vortex aerodynamic windows are designed. Solution of the problem starts with calculation of the flow quantities in the outlet section of the nozzle, based on which the nozzle contour is constructed. The initial flow quantities include the type of working gas (the ratio of specific heat capacities, γ, and the molar mass, μ), total temperature and total pressure (T_0 and p_0), static pressures in the separated streams (p_1 and p_2), and geometrical characteristics of the aerodynamic window (width d and jet turning angle δ). The design and geometry of the nozzle contours are shown in the Figure 1.

The problem is to design a nozzle that ensures a required distribution of the Mach number, M, and velocity ratio on the outlet boundary of the nozzle, $\zeta = v/u$. The nozzle outlet surface is set as a pressure outlet boundary. A stagnation inlet is used to replicate the experimental conditions of a high-pressure inlet. The stagnation inlet boundary requires representative total values for the pressure and temperature. The pressure outlet is an outflow boundary condition suitable for compressible and internal flows. The outflow pressure is set at atmospheric pressure. The standard wall condition, which represents a no-penetration surface, is used for the nozzle sides. As the simulations are inviscid, the slip wall condition is implicitly chosen.

The problem is solved in two steps.

Step 1. For the free vortex, the Mach number and the velocity ratio are found from

$$\mathrm{M} = \left[\frac{2}{\gamma - 1}\frac{1}{(r/r_\infty)^2 - 1}\right]^{1/2}, \quad \zeta = \frac{d}{2(r^2 - d^2/4)^{1/2}},$$

where $r \in [r_1, r_2]$. The external and internal radius of the vortex, r_1 and r_2, are found from

$$r_1 = \frac{d}{2\sin(\delta/2)}, \quad r_2 = r_\infty \left[1 + \frac{2}{(\gamma-1)\mathrm{M}_2^2}\right]^{1/2}.$$

The limiting radius of the vortex, r_∞, is found from

$$\frac{r_1}{r_\infty} = \left[1 + \frac{2}{(\gamma-1)\mathrm{M}_1^2}\right]^{1/2}.$$

The Mach numbers M_1 and M_2 are found from the isentropic relationships

$$\mathrm{M}_1^2 = \frac{2}{\gamma-1}\left[\left(\frac{p_1}{p_0}\right)^{-(\gamma-1)/\gamma} - 1\right], \quad \mathrm{M}_2^2 = \frac{2}{\gamma-1}\left[\left(\frac{p_2}{p_0}\right)^{-(\gamma-1)/\gamma} - 1\right].$$

The nozzle is designed using the diagram presented in the Figure ??, where $\xi \in [0, 1]$. The nozzle consists of two segments. The segment $A_1A_2B_2B_1$ in the vicinity of the nozzle throat is symmetric. Its shape is taken from the condition of smoothness ensuring a required technological simplicity. To construct the contour of this segment, circular arcs with the centers lying on the straight line intersection the inlet boundary are used. On the inlet segment, the flow is accelerated to small supersonic velocities. To construct the contour of the segment $A_2A_5B_5B_2$, Bezier curves are applied. The lower contour of the nozzle is constructed from the points A_2, A_3, A_4 and A_5, and the upper contour of the nozzle is constructed from the points B_2, B_3, B_4 and B_5. This segment forms the required distribution of the flow quantities on the outlet boundary.

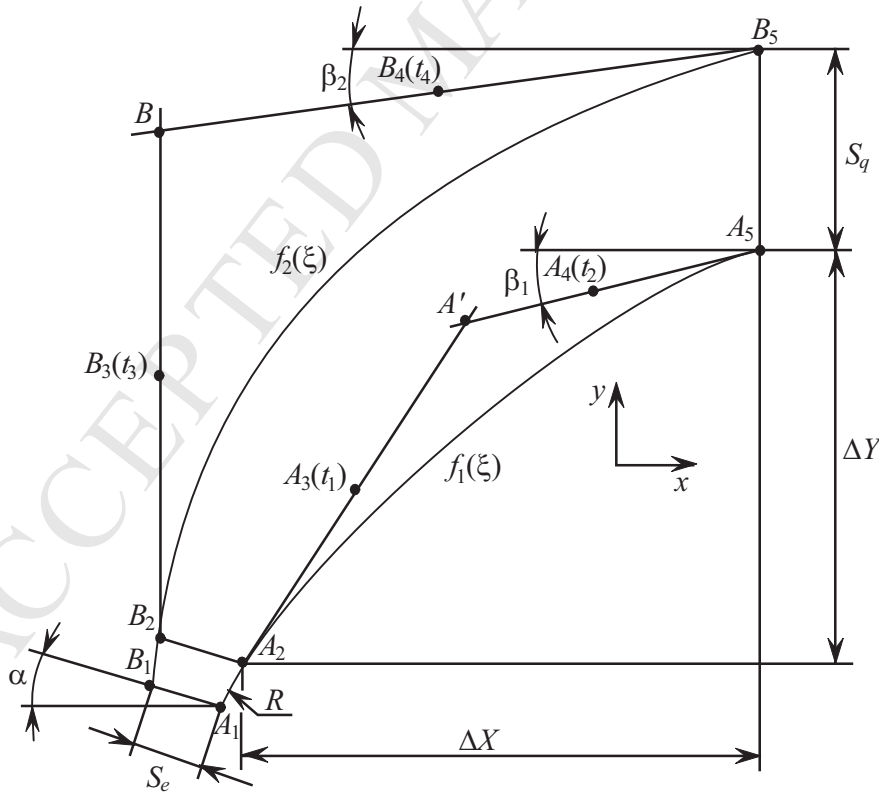

Figure 12. Nozzle profiling

Step 2. The area of the outlet nozzle boundary is found from the geometrical considerations

$$S_q = \left(r_2^2 - \frac{d^2}{4}\right)^{1/2} - \left(r_1^2 - \frac{d^2}{4}\right)^{1/2}.$$

The area of the inlet nozzle cross section is found from the mass flow rate ratio which is equal to the mass flow rates through the throat and outlet boundary

$$S_e = \int_0^{S_q} \frac{q(\mathrm{M})}{(\zeta^2+1)^{1/2}} ds,$$

where

$$q(\mathrm{M}) = \left(\frac{\gamma-1}{2}\right)^{(\gamma+1)/[2(\gamma-1)]} \left(1+\frac{\gamma-1}{2}\mathrm{M}^2\right)^{(\gamma+1)/[2(\gamma-1)]} \mathrm{M}.$$

Angles β_1 and β_2 are found from the condition that the flow is tangential to the wall

$$\beta_1 = \mathrm{atan}[\zeta(r_1)], \quad \beta_2 = \mathrm{atan}[\zeta(r_2)].$$

The remaining eight parameters determining the nozzle contour include the angle of inclination of the inlet boundary to the centreline, α; the radius of the circular arcs on the first segment of the nozzle, R; the coordinates of the position of the outlet boundary relative to the point A_2 (ΔX and ΔY); the parameters determining the position of the points A_3, A_4, B_3 and B_4 (t_1, t_2, t_3 and t_4). The required flow quantities in the outlet boundary are found by varying the values of these parameters. The target function is

$$\sigma = \sigma(\alpha, R, \Delta X, \Delta Y, t_1, t_2, t_3, t_4).$$

The discrepancy between the flow quantities and the required values is determined by the function

$$\sigma = \sum \left[\psi \left(\frac{\Delta \mathrm{M}_i}{\Delta \mathrm{M}_{\max}}\right)^2 + (1-\psi)\left(\frac{\Delta\zeta_i}{\Delta\zeta_{\max}}\right)^2\right],$$

where $\psi \in [0,1]$ is the weighting factor. The typical convergence criteria (continuity, momentum and energy residuals) are monitored against iteration. Convergence is deemed attained when the residuals have achieved a stable value.

The challenge is to find the flow quantities α, R, ΔX, ΔY, t_1, t_2, t_3 and t_4 at which the angle α reaches the minimum ($\sigma \to 0$). Designing the nozzle contour leads to a problem of parametric optimization whose solution is found with the gradient method. Derivatives necessary for calculations are found by solution of gas dynamic problems with basic and increment values. Flow in the supersonic nozzle is calculated using the space-marching method. On the inlet boundary, the Mach number is close to unity (M = 1.005). Initial data for the parametric optimization are $p_1 = 5\times10^3$ Pa, $p_2 = 10^5$ Pa, $p_0 = 10^6$ Pa, $T_0 = 300$ K, $d = 40$ mm, $\delta = 5.768°$. Air ($\gamma = 1.4$, $\mu = 0.029$ kg/mol) is used as the working gas.

The initial nozzle contour and the distribution of Mach number on the outlet boundary are shown in the Figure 13. The solid and dashed lines correspond to the required distribution of the Mach number and to the Mach number distribution on the first iteration of the optimization loop. The maximum disagreement between the calculated and required Mach numbers is $\Delta\mathrm{M} = 1.135$. The maximum disagreement between the calculated and required Mach number is reduced to $\Delta\mathrm{M} = 0.086$ at the end of the optimization loop. The final results are shown in the Figure 14 where $\Delta\mathrm{M} = 0.036$. The density contours in the jet at the end of optimization loop are shown in the Figure 15.

Figure 13 and Figure 14 compare flows formed when a uniform flow and a free-vortex flow enter the diffuser. The jet with a velocity distribution corresponding to the free vortex

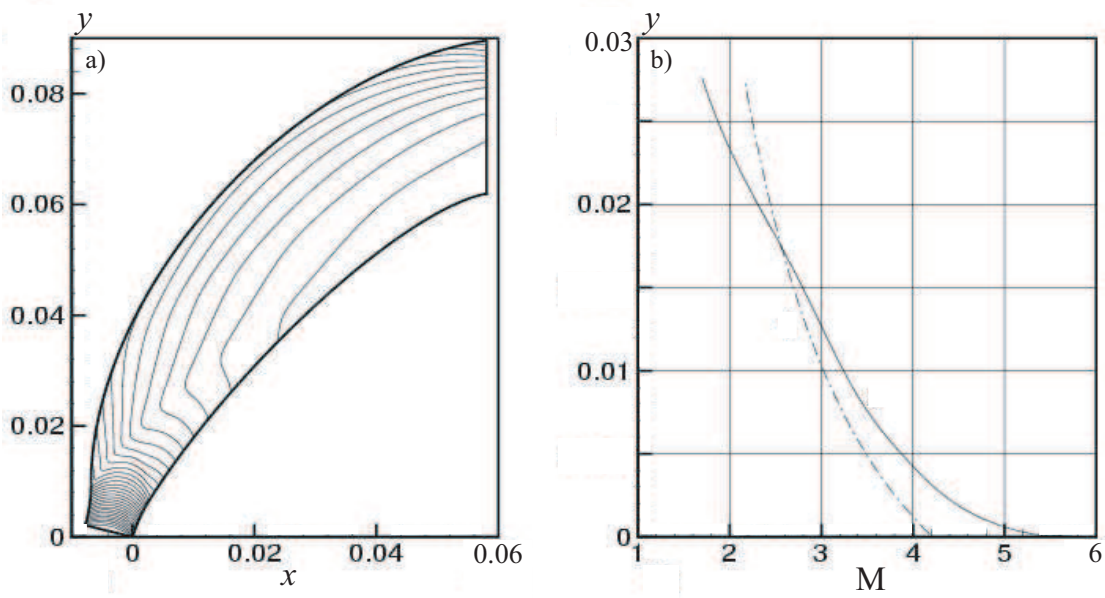

Figure 13. Density contours (a) and distributions of Mach number (b) at the nozzle outlet on the first iteration

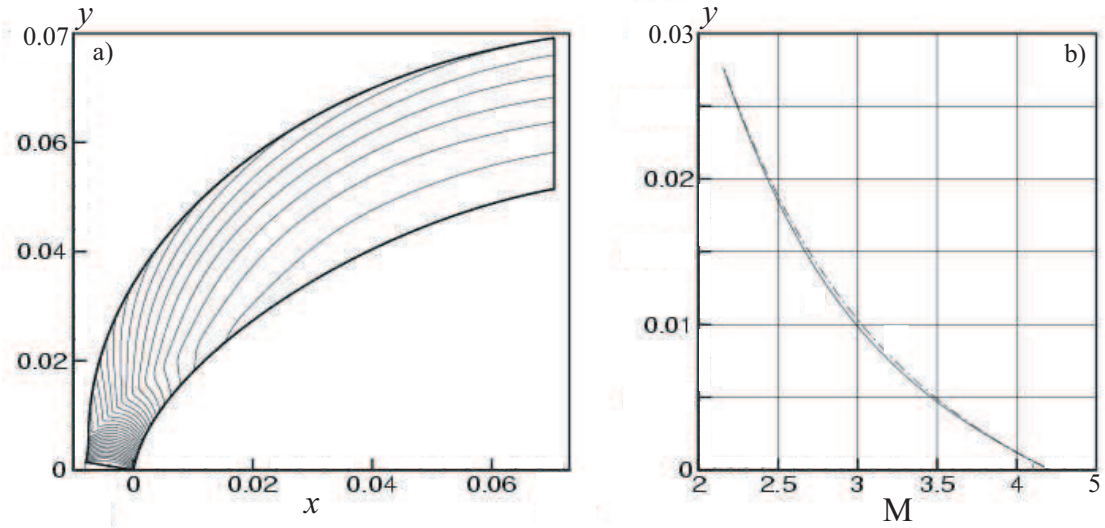

Figure 14. Density contours (a) and distributions of Mach number (b) at the nozzle outlet on the last iteration

is incident on a rectilinear channel, rarefaction waves and shocks are formed in the channel flow despite the fact that the flow is parallel to the channel walls on the inlet boundary.

The free-vortex aerodynamic window is designed to operate at an ambient pressure to cavity pressure ratio of 10. The pressure support characteristic for the aerodynamic window is established by determining the ambient to cavity pressure ratio over a range of aerodynamic window supply pressures. The lower wall of the diffuser is plane, and the upper wall is inclined to the horizontal axis. Parallel displacement of the upper wall of the diffuser in the vertical direction leads to variation in pressure ratio. The location of the upper wall is defined by the non-dimensional parameter $\overline{c} = c/h$, where c is the distance between original ($c = 0$) and modified positions ($c \neq 0$) of the upper wall, h is the width of the diffuser channel (Figure 1).

The aerodynamic performance of the window is evaluated in terms of the simulated laser cavity pressure and plenum pressure of the free-vortex supply nozzle. The aperture

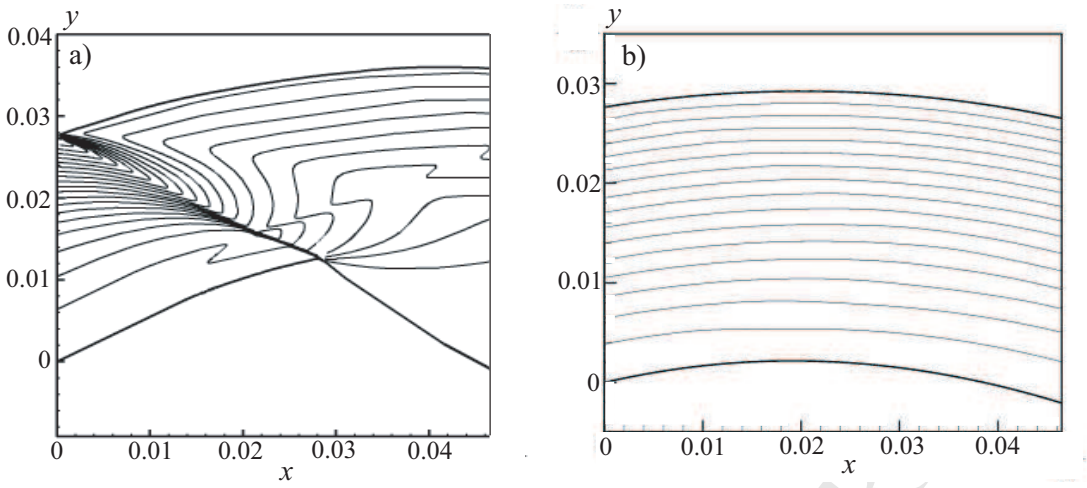

Figure 15. Density contours in the free-vortex jet on the first iteration (a) and density contours in the free-vortex jet on the last iteration (b)

dimension is 40 mm, the jet turning angle is 60 degrees, Mach numbers on the cavity side and atmospheric side are 3.71 and 2.12, and the mass flow rate is 3.02 kg/s. The Figure 16 shows the dependency of the cavity pressure on the plenum pressure, where $\overline{p} = p_u/p_l$ is the ratio of static pressures on upper and lower sides, $\overline{p}_0 = p_0/p_u$ is the relative total pressure of working gas (ratio of total pressure in the plenum and static pressure on upper side). The calculations give that $\overline{p}_0 = 9.8$ and $\overline{p} = 8.4$. The cavity pressure decreases monotonously with increasing plenum pressure. Variation of the non-dimensional displacement of the lower diffuser wall, $\overline{c}$, from 0.28 to 1.55 leads to increase in pressure ratio, $\overline{p}$, from 2 to 4.2 (for on-design conditions, $\overline{p}_0 = 8$ and $\overline{p} = 2$). The position of the upper wall of the diffuser has a small impact on the pressure ratio.

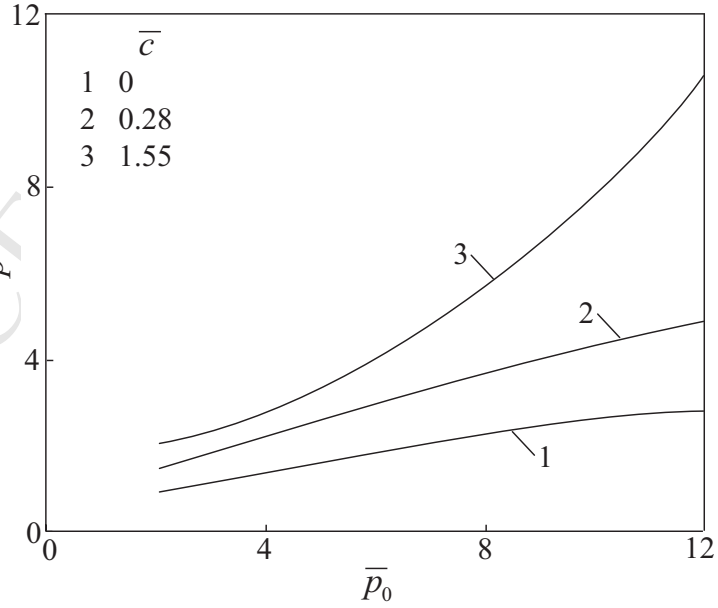

Figure 16. Dependency of the cavity pressure on plenum pressure for different locations of the lower diffuser wall

7 Conclusion

High-speed flows significantly affect the performance and robustness of optical sensors and optical windows, and simulation of high-speed flows becomes important in terms of evaluation of the structure of compressible flow and aerodynamic heating of the window material inducing large density gradients on a shock wave in front of the optical window.

The extraction of a laser beam from the cavity of a high-power gas laser through a solid window is difficult due to large density gradients in the compressible flow and excessive heating of the window material by the absorbed laser beam. Aerodynamic windows use the momentum of a supersonic jet to support the pressure difference between the laser cavity and the ambient atmosphere permitting the extraction of the laser beam through a non-absorbing gas. Optimization of the flowfield in a jet flow and nozzle profiling allow to increase the pressure ratio of the aerodynamic window and reduce mass flow rate of the working gas. The free-vortex aerodynamic window takes advantage of the centripetal force of the free-vortex motion of fluid. Free-vortex aerodynamic windows are most economic from a point of working gas consumption and large pressure differences.

The proposed model, numerical method and computational algorithm allow to design jets and nozzles of the aerodynamic windows of gas lasers with required distributions of flow quantities. Viscous effects that cause detachment, jet spreading and boundary layer growth make a real behavior significantly different from the model solutions far downstream of the nozzle outlet and prevent any accurate quantitative data from being attained. Skewing the initial velocity profile allows to eliminate expansion and turning shock waves.

Acknowledgements

This work was financially supported by the Ministry of Education and Science of Russian Federation (agreement No 14.577.21.0277, unique identifier of applied scientific research RFMEFI57717X0277).

References

[1] Smirnov N.N., Kiselev A.B., Smirnova M.N., Nikitin V.F. Space traffic hazards from orbital debris mitigation strategies. Acta Astronautica, 2015, 109, 144–152.

[2] Betelin V.B., Smirnov N.N., Nikitin V.F. Supercomputer predictive modeling for ensuring space flight safety. Acta Astronautica, 2015, 109, 269–277.

[3] Kremeyer K.P. Energy deposition I: applications to revolutionize high speed flight and flow control. AIAA Paper, 2015, 2015-3560 (14 pages).

[4] Kremeyer K.P. Energy deposition II: physical mechanisms underlying techniques to achieve high-speed flow control. AIAA Paper, 2015, 2015-3502 (16 pages).

[5] Boreisho A.S. High-power mobile chemical lasers. Quantuum Electronics, 2005, 35(5), 393–406.

[6] Parmentier E.M. Supersonic flow aerodynamic windows for high power lasers. AIAA Paper, 1972, 72-710 (12 pages).

[7] Parmetier E.M., Greenberg R.A. Supersonic flow aerodynamic windows for high-power lasers. AIAA Journal, 1973, 11(7), 946–949.

[8] Efremov N.M., Tikhonov B.A. An experimental study of gas dynamic windows for gas lasers. Fluid Dynamics, 1977, 12(2), 329–332.

[9] Behrens H.W., Shwartz J., Kulkarny V.A. Beam quality of continuous and pulsed axial aerodynamic windows. Proceedings of SPIE, Laser Diagnostics, 1982, 343 (16 pages).

[10] Khailov V.M., Shelomovskii V.V. Aerodynamic window with a pressure separation ratio greater than 500. Journal of Engineering Physiccs and Thermophysics, 1991, 61(6), 1492–1496.

[11] Guile R.N., Mapes S.N., Director M.N., Coulter L.J. Performance of a multi-element centrifugal aerowindow. AIAA Paper, 1974, 74-227 (10 pages).

[12] Guile R.N., Hilding W.E. Investigation of a free-vortex aerodynamic window. AIAA Paper, 1975, 75-122 (10 pages).

[13] Masuda W., Yuasa M. Experimental study of a free-vortex aerodynamic window. Journal de Physique, 1980, 41(11), 423–429.

[14] Wildermuth E., Giesen A., Hűgel H. Experimental investigations of a free-vortex aerodynamic window. Proceedings of the 6th International Symposium on Gas Flow and Chemical Lasers, 8–12 September 1986, Jerusalem, Israel. Springer, 1987, 96–100.

[15] Sonoda K., Ohira K., Nanba K., Wada T. Research of supersonic free-vortex aerodynamic window: design procedure of free vortex nozzle and operating condition. Transactions of the Japan Society of Mechanical Engineers B, 1996, 62(599), 2687–2694.

[16] Satake T., Sakai M., Watanabe T., Nakajima M., Horioka K. Experimental investigation of supersonic free-vortex flow with large asymmetry for aerodynamic laser windows. Japanese Journal of Applied Physics, 1998, 37(8), 4377–4382.

[17] Boreisho A.S., Trilis A.V., Khailov V.M., Sericov R.I. Improvement of the optical quality of the free-vortex aerodynamic windows. Proceedings of SPIE, Laser Optics, 2001, 4351 (12 pages).

[18] Malkov V.M., Trilis A.V., Savin A.V., Druzhinin S.L. One-stage free-vortex aerodynamic window with pressure ratio 100 and atmospheric exhaust. Proceedings of SPIE, 2005, 5777 (10 pages).

[19] Emelyanov V.N., Teterina I.V., Volkov K.N., Yakovchuk M.S. Aero-optical effects in free and wall-bounded turbulent compressible flows. Acta Astronautica, 2018, 150, 144–152.

[20] Liu L., Meng W., Li Y., Dai X., Zuo Z. Influence of aero-optical transmission on infrared imaging optical system in the supersonic flight. Infrared Physics and Technology, 2015, 68, 110–118.

[21] Kraiko A.N., Shelomovskii V.V. On profiling planar and axisymmetric nozzles and channels to achieve a given supersonic stream at the exit section. Fluid Dynamics, 1981, 16(4), 564–572.

[22] Karamyshev V.B. An approach to the construction of marching algorithms for stationary problems of gas dynamics. Computational Mathematics and Mathematical Physics, 1992, 32(10), 1507–1508.

[23] Yamaleev N.K., Ballmann J. Space-marching method for calculating steady supersonic flows on a grid adapted to the solution. Journal of Computational Physics, 1998, 146(1), 436–463.

[24] Zapryagaev V., Kiselev N., Gubanov D. Shock-wave structure of supersonic jet flows. Aerospace, 2018, 5, 60 (18 pages).

[25] Silnikov M.V., Chernyshov M.V., Uskov V.N. Two-dimensional over-expanded jet flow parameters in supersonic nozzle lip vicinity. Acta Astronautica, 2014, 97, 38–41.

[26] Silnikov M.V., Chernyshov M.V., Uskov V.N. Analytical solutions for Prandtl–Meyer wave – oblique shock overtaking interaction. Acta Astronautica, 2014, 99, 175–183.

[27] Silnikov M.V., Chernyshov M.V. Incident shock strength evolution in overexpanded jet flow out of rocket nozzle. Acta Astronautica, 2017, 135, 172–180.

[28] Jegede O.O., Crowther W.J. Low order supersonic nozzle design using superimposed characteristics. AIAA Paper, 2016, 2016-0805 (13 pages).

[29] Ashrafizadeh A., Raithby G.D., Stubley G.D. Direct design of ducts. Journal of Fluids Engineering, 2003, 125(1), 158–165.

Supersonic jet and nozzle flows in uniform-flow and free-vortex aerodynamic windows of gas lasers

V.N. Emelyanov[1], A.V. Pustovalov[1], K.N. Volkov[2]

[1]Faculty of Rocket and Space Engineering, Baltic State Technical University, 190005, St. Petersburg, Russia
[2]Faculty of Science, Engineering and Computing, Kingston University, SW15 3DW, London, United Kingdom

- Simulation of supersonic jet flows in aerodynamic windows is performed
- Results are presented for under-expanded and over-expended jets
- Aerodynamic performance is evaluated for free-vortex supply nozzle
- Study provides information for design of aerodynamic windows